THE JOURNAL OF PHYSICAL CHEMISTRY C

Article

pubs.acs.org/JPCC

Efficient Approach for the Computational Study of Alcohol and Nitrile Adsorption in H-ZSM-5

Jeroen Van der Mynsbrugge, Karen Hemelsoet, Matthias Vandichel, Michel Waroquier, and Veronique Van Speybroeck*

Center for Molecular Modeling, Ghent University, Technologiepark 903, 9052 Zwijnaarde, Belgium and QCMM Alliance, Ghent-Brussels, Belgium

Supporting Information

ABSTRACT: Since many industrially important processes start with the adsorption of guest molecules inside the pores of an acidic zeolite catalyst, a proper estimate of the adsorption enthalpy is of paramount importance. In this contribution, we report ab initio calculations on the adsorption of water, alcohols, and nitriles at the bridging Brønsted sites of H-ZSM-5, using both cluster and periodic models to account for the zeolite environment. Stabilization of the adsorption complexes results from hydrogen bonding between the guest molecule and the framework, as well as from embedding, i.e., van der Waals interactions with the pore walls. Large-cluster calculations with different DFT methods, in particular B3LYP(-D), PBE(-D), M062X(-D), and ωB97X-D, are tested for their ability to reproduce the experimental heats of adsorption available in the literature (*J. Phys. Chem. B* **1997**, *101*, 3811−3817). A proper account of dispersion interactions is found to be crucial to describe the experimental trend across a series of adsorbates of increasing size, i.e., an increase in adsorption enthalpy by 10−15 kJ/mol for each additional carbon atom. The extended-cluster model is shown to offer an attractive alternative to periodic simulations on the entire H-ZSM-5 unit cell, resulting in virtually identical final adsorption enthalpies. Comparing calculated stretch frequencies of the zeolite acid sites and the adsorbate functional groups with experimental IR data additionally confirms that the cluster approach provides an appropriate representation of the adsorption complexes.

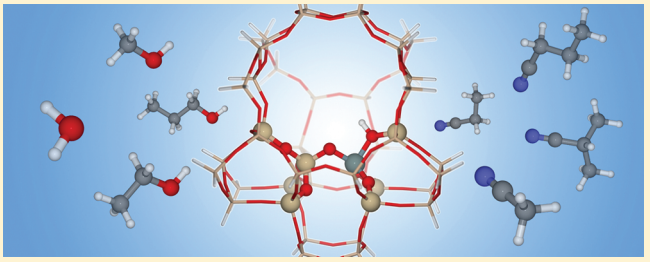

1. INTRODUCTION

Catalytic conversions on acidic zeolite catalysts are applied in a whole range of industrial production processes.[1] In recent years, theoretical modeling has been proven a highly useful tool to complement experimental studies in gaining a deeper understanding of the complex reaction mechanisms taking place inside the zeolite pores. Theoretical simulations allow obtaining information about individual reaction steps, which is highly difficult to achieve through experiments, due to many side reactions occurring simultaneously. A prominent example is the methanol-to-olefin process (MTO).[2,3] Several computational studies have provided invaluable insights into the catalytic cycles responsible for olefin production[4−9] and the origin of catalyst deactivation.[10,11] While earlier studies were primarily aimed at obtaining a better mechanistic insight, current research efforts tend to focus on developing efficient theoretical procedures to accurately predict experimentally observed reaction barriers and rate coefficients.[12,13] Experimental studies typically start from gas phase reactants that diffuse into the zeolite pores and adsorb onto the active sites before undergoing reaction. A proper estimate of the initial heat of adsorption is therefore necessary for the precise theoretical description of an entire reaction path.[12,13]

In this work, a set of adsorbate molecules were selected for which experimentally determined differential heats of adsorption on H-ZSM-5 are available.[14] The test set (Figure 1) consists of water, primary alcohols (methanol, ethanol, and propanol), and nitriles (acetonitrile, propionitrile, butyronitrile, and isobutyronitrile), all of which preferentially interact through hydrogen bonds with the Brønsted acid sites inside the zeolite. If these acid sites are sufficiently isolated, well-defined complexes of one adsorbate molecule per active site will be formed. These adsorption complexes are additionally stabilized by dispersive interactions with the pore walls, resulting in an increase in adsorption enthalpy of 10−15 kJ/mol for each additional carbon atom.[14] A similar effect has been

H–OH	CH_3–C≡N
CH_3–OH	CH_3–CH_2–C≡N
CH_3–CH_2–OH	CH_3–$(CH_2)_2$–C≡N
CH_3–$(CH_2)_2$–OH	$(CH_3)_2$–CH–C≡N

Figure 1. Adsorbate molecules considered in this study: water, methanol, ethanol, propanol, acetonitrile, propionitrile, butyronitrile, and isobutyronitrile.

Received: December 22, 2011
Revised: February 7, 2012
Published: February 10, 2012

reported for the adsorption of *n*-alkanes and *n*-alkenes in different zeolites; the adsorption enthalpy was found to increase by 10−12 kJ/mol per carbon atom, depending on the zeolite topology, the silicon−aluminum ratio, and the temperature.[15−18]

At 400 K, primary alcohols and nitriles are fairly unreactive, such that accurate adsorption enthalpies can be obtained from calorimetric measurements,[14] which are ideally suited as reference data for a theoretical benchmarking study. Furthermore, our selection comprises two series of structural analogues with identical functionality, enabling a systematic investigation of the different contributions to the adsorption enthalpy with increasing adsorbate size.

As long-range interactions and topological characteristics of the zeolite are of paramount importance to the stabilization of various adsorbates, computational models need to take the zeolite framework into account. Many current studies on adsorption and/or catalysis in zeolites employ methods with periodic boundary conditions to treat the complete system.[13,17−25] However, rate coefficients and barriers for methylation reactions have been successfully predicted using an extended-cluster model in which only a fragment of the zeolite structure is considered.[12] Provided the selected fragment is large enough, the cluster approach allows accounting for all relevant confinement effects. Besides a better computational efficiency, cluster calculations have the additional advantage over periodic simulations that the vibrational analysis is much more straightforward, which is vital for the calculation of thermodynamic properties and kinetic coefficients.

In both finite-cluster and periodic studies, density functional theory (DFT) methods[26,27] are nowadays frequently used; they offer a favorable balance between accuracy and computational efficiency and can therefore be applied to large systems of chemical relevance. A serious drawback, however, is their lack of a proper description of long-range electron correlation effects that cause dispersive or van der Waals interactions.[28,29] Previous studies have shown that neglecting these van der Waals interactions has only a limited effect on intrinsic barriers (about 10−20 kJ/mol), such that the general picture of reaction routes determined with standard DFT methods (e.g., the popular B3LYP functional[30,31]) remains largely unaltered for most reactions, although one must be careful when generalizing this conclusion.[7,8,10] This is no longer the case for adsorption steps, for which the effect of dispersive interactions can become highly significant and may result in differences in adsorption energy of up to 70 kJ/mol.[12,13,19]

Many efforts have been made in recent years to include van der Waals interactions within the framework of DFT, allowing a substantial decrease in computational expense.[32−35] Several of these methods will be employed in this paper and are briefly highlighted.

One of the most effective and most widely applied methods, is the so-called DFT-D scheme proposed by Grimme[28,36,37] In this method, an empirical damped-potential term is added to energies obtained with standard functionals, at a negligible computational cost. Since its first introduction, the DFT-D method has been successfully applied on a wide variety of systems, demonstrating its robustness.[37] In the latest version (referred to as DFT-D3), ab initio data have to a large extent replaced the empirical input, such that dispersion corrections are now available for all elements, with improved overall performance.[37]

Other attempts to include dispersive interactions involve developing new functionals which are specifically parametrized for systems in which weak interactions play a prominent role. The most well-known example of such a functional is found in the M06 family, developed by the Truhlar group.[38,39] In the hybrid M06−2X functional, double Hartree−Fock exchange is included to improve the description of noncovalent interactions. Successful applications of this functional include the study of π-stacking interactions on aromatic systems.[40,41] Recently, M06−2X has also been employed to investigate zeolite-catalyzed reactions.[42,43]

While the DFT-D approach proposed by Grimme has the advantage of allowing us to improve the results obtained with commonly used DFT methods without changing the original functionals, the addition of the separate dispersion term to the regular DFT energy can lead to some amount of double-counting of total energy in the intermediate range. This can be avoided by self-consistently parametrizing dispersion-corrected functionals in their entirety. Examples of this approach include Grimme's B97-D functional[44] and Chai and Head-Gordon's ωB97X-D functional.[45] The latter is a long-range corrected hybrid density functional, which was reoptimized to include dispersion corrections. A recent benchmarking study by Goerigk and Grimme on an extensive database dubbed GMTKN30 found the ωB97X-D functional to be a promising method for main group thermochemistry, kinetics, and noncovalent interactions.[35]

All investigated adsorbate molecules (Figure 1) are weak bases, which makes them attractive probe molecules for zeolite acidity since their interactions with the Brønsted acid sites cause measurable shifts in the vibrational spectra.[46] Thus far, a lot of attention was given to the issue whether in different zeolite systems the adsorbed complex is physisorbed (hydrogen bonded) or chemisorbed. The interpretation of experimental IR spectra based on theoretical simulations has overall been subject to debate as it turns out that the final outcome depends on both the applied theoretical procedure and the model. In this context, mainly water and alcohol adsorption have been examined.[47−51] Experimental IR spectra of the smallest investigated compounds, i.e., water,[52] methanol,[53] ethanol,[54] and acetonitrile[55−59] adsorbed in H-ZSM-5, are available, which can be compared to theoretical values to further validate proposed models. The assignment of the various bands has proven challenging, and several studies focused on the observed (A,B,C) triplet of infrared OH bands around 2800, 2400, and 1700 cm^{-1}.[46,52,53] In the case of acetonitrile, theoretical computations of the IR spectra can serve as a useful tool to discuss acid−base interactions. Pelmenschikov pointed out that the CN stretching frequency is an efficient probe to distinguish different adsorption sites in zeolites, in particular Lewis acid sites, terminal silanol groups, and the bridging Brønsted acid site, which will be discussed in this work.[55,56] Related work of Simperler et al. obtained a ranking of seven different high silica zeolites based on the hydrogen-bond strength as a predictor of acidity.[60] In this study, the shift in the ν(OH) region will be investigated for all adsorption complexes. For the nitrile series, the ν(CN) frequency will also be examined.

In this paper, the adsorption of the selected alcohols and nitriles in H-ZSM-5 is studied using both cluster and periodic models. The cluster approach will be combined with different contemporary DFT methods to test their ability to account for dispersion. A complete vibrational analysis will enable the calculation of adsorption enthalpies at 400 K, which are directly

dx.doi.org/10.1021/jp2123828 | J. Phys. Chem. C 2012, 116, 5499−5508

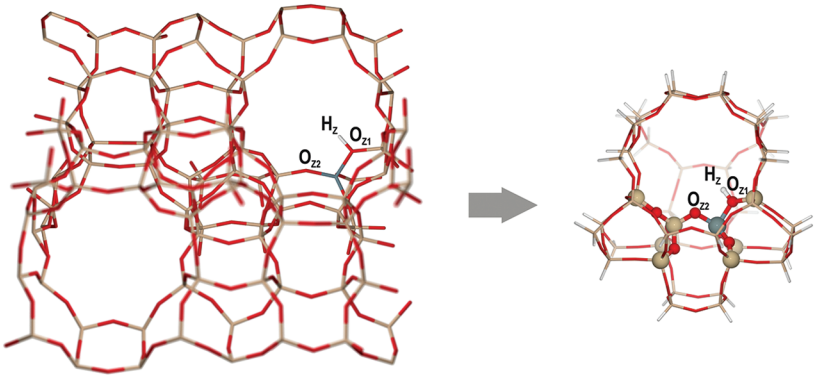

Figure 2. Theoretical model for the H-ZSM-5 catalyst. The aluminum defect is located at the T12 position. The full periodic structure (left) is reduced to an extended cluster model containing 46T atoms (right). In ONIOM calculations, a central 8T fragment of the catalyst (indicated in ball-and-stick representation) is included in the high-level region.

comparable to the experimentally measured values.[14] Investigation of characteristic IR frequencies and comparison with available experimental data will help to validate whether realistic representations of H-ZSM-5 at low loadings of weak bases can be obtained using the cluster model. Additionally, adsorption enthalpies are calculated based on the periodic simulations in which the entire unit cell is taken into account and compared to those obtained from the cluster approach.

2. ZEOLITE MODELS AND COMPUTATIONAL METHODS

2.1. Selection of the Brønsted Acid Site. In this study, we focus on a single active site within an H-ZSM-5 catalyst to investigate the adsorption complexes formed at low coverages. The zeolite model is constructed by introducing an aluminum defect at the T12 crystallographic position of an orthorhombic MFI unit cell.[61] This position, at the intersection of the straight and sinusoidal channels, offers maximum available space and creates the most accessible active site to accommodate various guest molecules.[62,63] While several studies[64−67] have attempted to determine the most favorable position for aluminum substitution, ultimately little preference for any specific position was found, and a distribution of T-sites hosting aluminum defects can be expected in a realistic zeolite crystal.[63] Additionally, recent experimental and theoretical evidence has confirmed that the framework position of aluminum defects and their distribution throughout the material is determined by kinetic effects occurring during zeolite synthesis, rather than on thermodynamic grounds.[68−70]

In this paper, the acidic proton H_Z is located on the bridging oxygen O_{Z1} (Figure 2), as in our previous work. The proton is well-known to easily migrate from one oxygen bridge to another,[71,72] especially when aided by assisting adsorbate species such as, e.g., water molecules.[73] However, a detailed investigation of all possible Brønsted sites would require a molecular dynamics approach, which is clearly beyond the scope of the current study and which is currently still limited by the lack of force-field methods offering the required accuracy for both host and guest species.

2.2. Cluster Calculations. In the majority of the calculations presented in this work, a large cluster model was used to represent the zeolite catalyst. A fragment containing 46 tetrahedral atoms (46T) was cut from the crystallographic structure, such that the model includes a sufficiently large portion of the framework surrounding the active site to account for relevant confinement effects (Figure 2).

Dangling bonds at the cluster edges were saturated with hydrogen atoms (Si−H termination). The terminating hydrogens were fixed in space to avoid unrealistic deformations of the cluster throughout geometry optimizations. Stationary points were localized using a two-level ONIOM scheme, in which a central 8T cluster is treated at the B3LYP/6-31+g(d) level of theory, while the remainder of the system is described using the semiempirical MNDO method. In a subsequent step, the energies were further refined by single-point calculations on the optimized structures. Full DFT calculations on the complete 46T cluster were performed at the B3LYP/6-31+g(d), M06−2X/6-31+g(d), ωB97X-D/6-31+g(d), and PBE/6-31+g(d) levels of theory. Dispersion corrections according to Grimme were added to the B3LYP, M06−2X, and PBE energies.[37,44] All cluster calculations were performed using the Gaussian03 and Gaussian09 packages,[74,75] and Grimme corrections were calculated with the dftd3 program available from the authors' Web site.[76]

2.3. Periodic Calculations. Periodic DFT-D calculations on the entire H-ZSM-5 unit cell containing 288 atoms (Figure 2) were carried out in the Vienna Ab Initio Simulation Package (VASP 5.2.11),[77−80] using the PBE exchange-correlation functional[81,82] and a plane-wave basis set with a general kinetic energy cutoff of 600 eV. The projector augmented wave (PAW) approximation[83] was used. Brillouin zone sampling was restricted to the Γ-point. Gaussian smearing[78] was applied to improve convergence: 0.05 eV for geometry optimizations, 0.03 eV for frequency calculations, and 0.005 eV for energy calculations on the optimized geometries. van der Waals corrections according to Grimme were used throughout all periodic calculations.[44]

The unit cell parameters of H-ZSM-5 were determined, starting from crystallographic data for silicalite,[84] using a similar procedure as Svelle et al.[13] The silicalite unit cell was fully optimized at the start but was also allowed to relax during subsequent geometry optimizations, i.e., after the aluminum defect, proton, and adsorbates had been introduced. Geometry optimizations of the adsorption complexes were carried out in two steps, similar to the approach proposed by De Moor et al.[25] An initial relaxation using the conjugate gradient algorithm was performed until the forces on all atoms are smaller than 0.01 eV/Å. This was followed by a second optimization with fixed cell parameters, in which the quasi-Newton algorithm is

dx.doi.org/10.1021/jp2123828 | J. Phys. Chem. C 2012, 116, 5499−5508

applied. Geometries are considered to be converged once the forces on the atoms drop below 0.005 eV/Å. For some of the adsorption complexes, even tighter criteria were required to eliminate all imaginary frequencies (cf. Section 2.4). Specific convergence criteria applied for each individual case are included in the Supporting Information (Table S1). The convergence criterion for the electronic self-consistent field (SCF) problem was set to 10^{-8} eV.

2.4. Normal-Mode Analysis and Thermochemistry. A normal-mode analysis was performed to verify the nature of the optimized structures (true energy minima should only have real frequencies) for both the cluster and periodic calculations, using Partial Hessian Vibrational Analysis (PHVA), as implemented in the in-house developed postprocessing toolkit TAMKIN.[85,86] In the cluster calculations, PHVA was used to exclude the terminating hydrogen atoms with constrained positions from the analysis. In the periodic calculations, vibrational modes are calculated numerically (using displacements in x, y, and z-directions of ±0.01 Å), and only a partial Hessian was calculated to reduce the computational cost. PHVA was applied on the adsorbate and the 8T atoms from the zeolite framework that are included in the high-level region in the ONIOM calculations on the cluster model. The strong hydrogen bond interactions between the alcohol or nitrile and the zeolite justify the application of the "immobile adsorbate" method, in which only harmonic frequencies are considered.[17,18,25]

The vibrational analysis also supplies the necessary thermochemistry data to allow the calculation of theoretical adsorption enthalpies at 400 K, the temperature at which the experimental reference data were obtained.[14] The adsorption enthalpy was calculated by subtracting the enthalpies of the empty zeolite and the gas phase adsorbate from the enthalpy of the adsorption complex

$$\Delta H_{ads} = H_{complex} - H_{zeolite} - H_{adsorbate}$$

Since we are using a flexible model[87] that is allowed to relax during geometry optimizations, in the cluster calculations the enthalpy of the empty zeolite was recalculated for each adsorbate, starting from the optimized geometry of the corresponding adsorption complex. The adsorbate molecule is removed from the complex, and the empty zeolite is subsequently optimized. This approach avoids nonreproducible errors on the calculated adsorption enthalpy caused by spurious enthalpy differences due to deformations of the zeolite host that are unrelated to interactions between the zeolite and the adsorbate under consideration.

IR spectra of all adsorption complexes were also investigated within the cluster model. Computed harmonic frequencies are typically larger than the experimentally observed values due to the neglect of anharmonic effects, the incomplete incorporation of electron correlation, and the use of a finite basis set. For this reason, a scale factor of 0.9648 was applied, which is common practice when using the B3LYP functional.[88]

3. RESULTS AND DISCUSSION

3.1. Geometrical Aspects of the Adsorption Complexes.

(A). Interaction with the Brønsted Acid Sites. At low coverages (up to one per active site), the investigated adsorbate molecules are known to form well-defined physisorption complexes at the Brønsted sites through hydrogen bonds; i.e., proton transfer between the zeolite and the adsorbates does not occur.[14] A complete overview of the critical distances and hydrogen bond angles in the adsorption complexes is included in the Supporting Information (Table S2).

Water and alcohols allow the formation of two hydrogen bond interactions with the active site, as the hydroxyl group can act simultaneously as hydrogen bond donor and acceptor (Figure 3a). In the cluster model the interaction between the zeolite proton (H_Z) and the oxygen atom of the hydroxyl group (O_A) results in a hydrogen bond of on average 1.52 Å. At the same time, the hydrogen end of the hydroxyl group (H_A) coordinates with a nearest-neighbor framework oxygen bridge with respect to the acid proton (O_{Z2}), resulting in a slightly longer hydrogen bond of about 1.89 Å. On the basis of the O–O distances ($d(O_A–O_{Z2}) \approx 2.72$ Å, $d(O_A–O_{Z1}) \approx 2.53$ Å), the hydrogen bonds can be classified as "strong" and "medium", respectively.[89] Clearly, the two hydrogen bonds could easily "switch places", thereby shuffling the acid proton between framework oxygen bridges. This observation is in agreement with previous theoretical results on the adsorption of methanol in zeolites by Sauer et al., which showed that complexes with methanol interacting in different configurations with the active site are very similar in energy and exist in a wide and shallow potential well. Ion-pair complexes in which the zeolite proton is fully transferred to methanol to form a methoxoniom ion were found to be slightly higher in energy, and these authors therefore considered them as transition states connecting different hydrogen bonded complexes.[20,73,90] In the periodic calculations performed in our current study, which included dispersion corrections throughout the optimizations, ion-pair complexes were obtained for methanol, ethanol and propanol, resulting in two fairly similar hydrogen bonds (average length 1.50 Å) between the protonated alcohol and two framework oxygens adjacent to the aluminum defect. Whether ion-pair complexes appear as stationary points or not most likely depends at least in part on the level of theory used. In particular, the addition of D-corrections and the kinetic energy cutoff might have an important influence on the result. Nguyen et al. recently reported both hydrogen bonded and protonated complexes for primary alcohols in H-ZSM-5, based on periodic PBE alculations using a cutoff energy of 400 eV.[22] In their study these authors included dispersion corrections as an energy refinement on the optimized geometries. More importantly, however, they also showed that the calculated adsorption

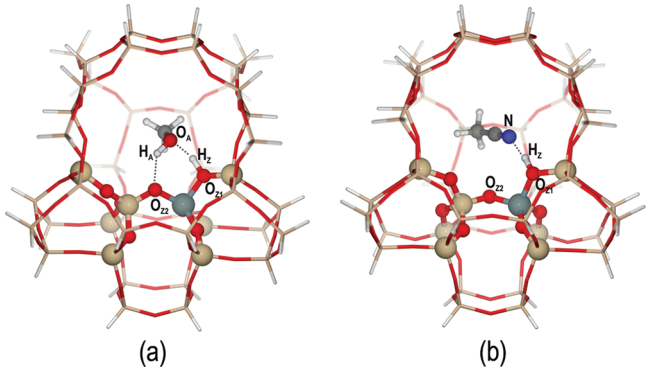

Figure 3. Hydrogen bond interactions with the Brønsted acid site in H-ZSM-5 in alcohol and nitrile adsorption complexes, e.g., methanol (a) and acetonitrile (b).

dx.doi.org/10.1021/jp2123828 | J. Phys. Chem. C 2012, 116, 5499–5508

energy is very similar for the neutral and ion-pair complexes, differing by less than 6 kJ/mol.[22]

In contrast, the nitriles can form only one hydrogen bond between the zeolite proton and the nitrogen end of the cyanide group, with an average length of about 1.66 Å in the cluster simulations (see Figure 3b). Consequently, these adsorbates cannot assist in transferring the zeolite proton to different positions in the framework. The final geometries obtained from the periodic calculations were very similar; the average length of the H_Z−N hydrogen bond was only slightly shorter, about 1.52 Å, which might again be due to the inclusion of dispersion corrections in the optimization.

(B). Orientation within the Zeolite Channels. In the gas phase, adsorbate molecules will preferentially assume conformations in which their carbon chains are fully staggered, thereby eliminating steric hindrance. Inside the zeolite pores, however, this might be prohibited by confinement effects, especially when larger adsorbates are concerned. While all adsorbates in the current study can still assume fully staggered conformations (cf. Figure S1 in Supporting Information), comparing the largest members of each series − propanol and butyronitrile − indicates that confinement effects will play a more important role with alcohols compared to nitriles (Figure 4). Larger nitriles can avoid steric hindrance by moving into the straight channel of the MFI structure. Alcohols, on the other hand, are more constrained by the double hydrogen bond interaction with the active site, such that larger ones will be forced to assume a more folded conformation to align their carbon chain with the straight channel.

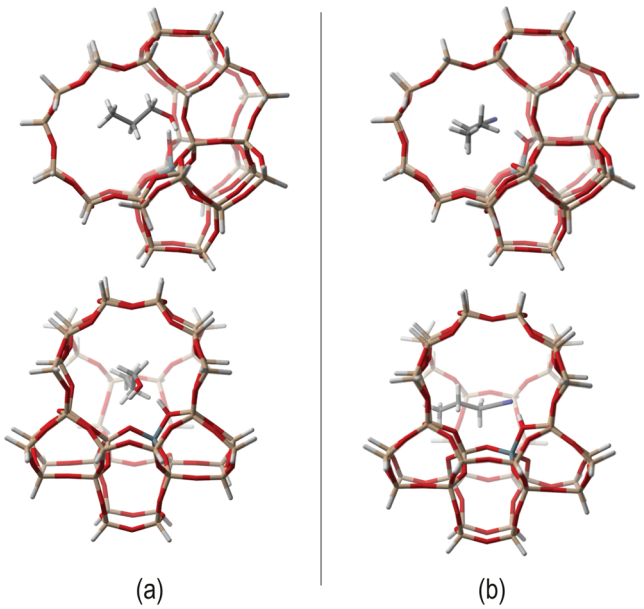

Figure 4. Optimized geometry of the adsorption complexes of propanol (a) and butyronitrile (b), viewed along sinusoidal (top) and straight (bottom) channels.

3.2. IR Spectroscopy. Calculated frequencies and relevant shifts resulting from adsorption of the weak bases are listed in Table 1. The scaled OH stretching frequency of the Brønsted acid site of the empty H-ZSM-5 cluster is on average 3600 cm^{-1}, in excellent agreement with reported experimental data (3610 cm^{-1}).[53] Upon physisorption of the bases, a clear red shift of the zeolite OH stretch (varying between 708 and 1360 cm^{-1}) is observed, due to the aforementioned hydrogen bonding. For a particular molecular type, the calculated shift roughly correlates with the proton affinity (PA) of the base, as depicted in Figure S2 (cf. Supporting Information). As a result, the red shift is the largest in the case of the alcohol series and increases with increasing molecular size. Comparison with available data for methanol adsorbed in H-ZSM-5 shows that the calculated shift of 1183 cm^{-1} (Table 1) is in good agreement with MP2-based results obtained on small cluster models of Haase and Sauer, reporting a shift of 1159 cm^{-1},[47] whereas periodic PBE simulations lead to a shift as large as 2233 cm^{-1}.[22] Notably, based on our large-cluster simulations the calculated OH stretch in adsorbed methanol equals 3426 cm^{-1}, which is in significantly better agreement with the experimentally reported[53] value of 3550 cm^{-1} compared to the MP2-based calculations using small clusters[47] and also to the PBE-based periodic simulations.[22]

For the nitrile series, several studies have reported on the influence of acetonitrile on the IR spectrum of initially unloaded H-ZSM-5.[55−59] The observed CN stretching frequency in the adsorption complex equals 2300 cm^{-1}, which is very well reproduced using our large-cluster approach (Table 1). Pelmenschikov et al.[55] reported calculated frequencies using small cluster models, and similar values were obtained. The shift of the CN stretch frequency in the adsorbed complex compared to the gas phase ranges from 9 to 24 cm^{-1}. The agreement with available data for acetonitrile is also satisfactory in this case (experimental shift equals 35 cm^{-1}[55]), suggesting that our theoretical model results in realistic structures for H-ZSM-5 at low loadings with weak bases.

3.3. Adsorption Enthalpy. For the complete series of adsorbate molecules, adsorption enthalpies at 400 K were calculated at the different levels of theory, as explained in Section 2.2. The majority of the calculations were performed using the extended-cluster model. To validate this approach, some additional fully periodic calculations were carried out. The final adsorption enthalpies obtained using the various methods are summarized in Table 2. Thermal corrections at 400 K are fairly similar for all adsorbates considered and add about +6 kJ/mol to the electronic energy differences. A complete breakdown of different contributions to the calculated adsorption enthalpies − i.e., electronic energies, dispersion corrections (where applicable), thermal corrections − is included in the Supporting Information (Table S3). Scatter plots depicting the correlation between calculated and experimental enthalpy values are shown in Figure 5.

First of all, adsorption enthalpies were calculated using the standard B3LYP functional. This functional does not include a proper description of dispersion interactions and was found to be completely inadequate for the calculation of adsorption enthalpies. The theoretical values predicted from the B3LYP energies significantly underestimate the experimental reference data[14] and are almost the same for all adsorbates considered, regardless of their size or chemical characteristics (Figure 5a). This is in complete contradiction with the experimental observation that across a series of similar compounds of increasing size (in this case alcohols or nitriles) the adsorption enthalpy increases steadily by about 10−15 kJ/mol with each additional C-atom in the carbon chain.[14] The outcome is significantly improved when D-corrections are added to the electronic energies: at the B3LYP-D level of theory, the experimentally observed trend in adsorption enthalpies is recovered across the series of alcohols and nitriles (Figure 5a).

dx.doi.org/10.1021/jp2123828 | J. Phys. Chem. C 2012, 116, 5499−5508

Table 1. Zeolite OH and Adsorbate CN Vibrational Stretching Frequencies in cm^{-1} for the Various Adsorption Complexes Obtained from Cluster Calculations[a]

	$\nu(O_{Z1}H_Z)$			ν(CN)		
	empty cluster[b]	adsorbed complex	shift	adsorbed complex	gas phase	shift
H_2O	3604	2687	917			
CH_3OH	3601	2418	1183			
CH_3CH_2OH	3602	2363	1239			
$CH_3(CH_2)_2OH$	3598	2238	1360			
CH_3CN	3600	2893	708	2307	2282	24
CH_3CH_2CN	3602	2845	757	2295	2271	24
$CH_3(CH_2)_2CN$	3597	2885	712	2280	2271	9
$(CH_3)_2CHCN$	3598	2809	790	2278	2263	15

[a]Frequencies are evaluated at the ONIOM(B3LYP/6-31+G(d):MNDO) level of theory. [b]The small differences result from the optimization of the empty cluster for all different adsorbates (see Section 2.4).

Table 2. Adsorption Enthalpies at 400 K Calculated Using Different DFT Methods, With and Without Dispersion Corrections (in kJ/mol)[a]

	B3LYP	B3LYP-D2	B3LYP-D3	M06−2X	M06−2X-D3	ωB97X-D	PBE	PBE-D2	PBE-D3	PBE-D2 pbc[b]	experimental[c]
H_2O	−71	−91	−90	−84	−88	−100	−80	−87	−91	−89	−90 ± 10
CH_3OH	−69	−108	−111	−93	−101	−102	−91	−108	−112	−125	−115 ± 5
CH_3CH_2OH	−82	−129	−132	−108	−120	−122	−97	−124	−129	−141	−130 ± 5
$CH_3(CH_2)_2OH$	−85	−148	−152	−119	−134	−139	−102	−140	−148		−145 ± 5
CH_3CN	−72	−104	−110	−89	−98	−101	−84	−102	−104	−108	−110 ± 5
CH_3CH_2CN	−72	−120	−127	−95	−108	−116	−87	−116	−120	−112	−120 ± 5
$CH_3(CH_2)_2CN$	−64	−137	−144	−105	−121	−130	−83	−128	−137	−139	−145 ± 5
$(CH_3)_2CHCN$	−69	−130	−139	−99	−115	−125	−86	−125	−130		−130 ± 5

[a]All cluster calculations were performed using the 6-31+g(d) basis set. [b]Periodic results obtained using a kinetic energy cutoff of 600 eV. [c]Experimental values from ref 14.

For completeness, we calculated dispersion corrections according to both the D2-scheme,[44] as used in our previous work,[11,12,91] and the more recent D3-version.[37] Overall, only minor differences were found between the two approaches.

Next, adsorption enthalpies were calculated based on M06−2X energies (Figure 5b). The numerical values show that, compared to B3LYP, some of the weak interactions between the zeolite host and the adsorbate molecule are accounted for by the M06−2X functional. However, the deviation from the reference data increases for the larger adsorbates, which is probably due to the specific way the M06−2X functional was parametrized. While this functional performs very well on systems with noncovalent interactions in the medium range, it does not possess the correct asymptotic behavior to describe long-range dispersion interactions.[35] The remaining deficiency can be remedied by adding an empirical dispersion correction term,[35] resulting in the recovery of the correct experimental trend. The M06−2X functional has recently been used for the study of zeolite-catalyzed processes.[42,43] However, our results reported in this paper indicate caution is required when using this method in cases for which dispersion interactions are important.

Subsequently, adsorption enthalpies were also evaluated using the ωB97X-D functional, resulting in a very good correlation with the experimental values (Figure 5c). This functional tends to predict a slightly lower interaction strength between adsorbate and zeolite compared to B3LYP-D, which can probably be ascribed to the simultaneous determination of all parameters in the ωB97X-D functional, thereby avoiding double counting in the intermediate range.[45] Although this functional has thus far not been used in the field, it could be a promising candidate for use in future research on zeolite-catalyzed reactions. Goerigk et al. reported on its good performance for main-group thermochemistry, kinetics, and noncovalent interactions based on a benchmarking study on the GMTKN30 database.[35] The performance of the ωB97X-D functional to describe the kinetics of methylation reactions is currently being investigated in our group.

Finally, enthalpies of adsorption were calculated based on fully periodic simulations in which the entire H-ZSM-5 unit cell is taken into account (see Section 2.3) to verify the validity of the extended-cluster model. To enable a direct comparison between periodic and cluster calculations, the PBE functional was used to evaluate adsorption enthalpies in both the cluster and periodic approach (Figure 5d). Considering only the cluster results, the qualitative performance of PBE appears similar to that of B3LYP, as it critically depends on the addition of dispersion corrections to recover the experimental trend across the series of adsorbates. Comparing periodic PBE-D with cluster PBE-D adsorption enthalpies, periodic simulations clearly do not offer a significant improvement over the cluster approach. Adsorption enthalpies for methanol and ethanol are predicted to be slightly larger by the periodic calculations, which could be related to protonated complexes being obtained for these adsorbates. For propanol and isobutyronitrile, no adsorption enthalpy at 400 K could be calculated, as even with the strong convergence criteria imposed the partial Hessian still contained imaginary frequencies. In general, the extended-cluster approach was found to offer a reliable alternative for the much more demanding periodic calculations, combining lower computational costs with less technical complications and a more straightforward vibrational analysis.

The overall performance of the different methods across the test set is summarized in Figure 6, displaying the mean

dx.doi.org/10.1021/jp2123828 | J. Phys. Chem. C 2012, 116, 5499−5508

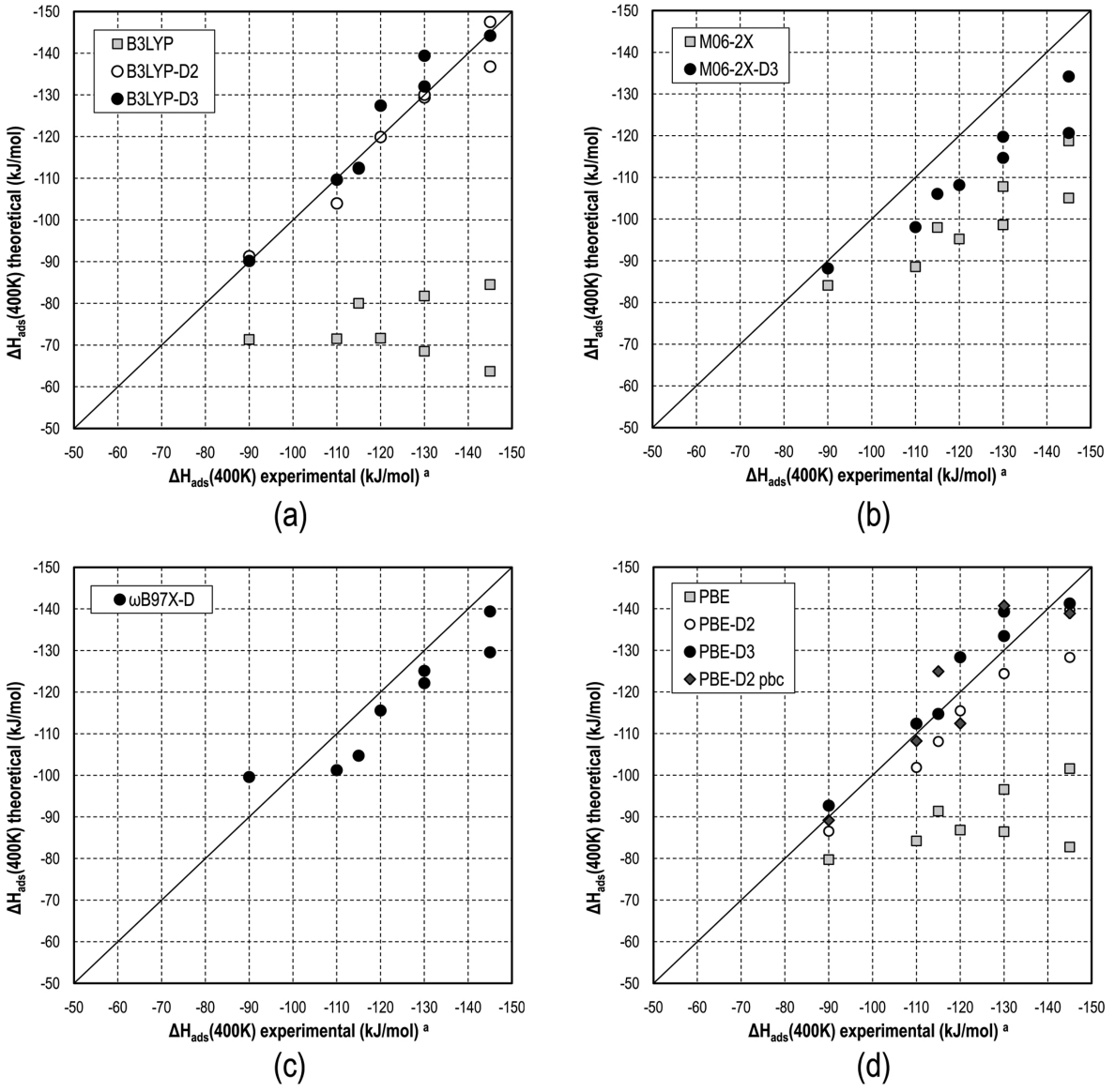

Figure 5. Correlation between theoretical (*y*-axis) and experimental (*x*-axis) values for adsorption enthalpies evaluated at different levels of theory: (a) B3LYP(-D), (b) M06−2X(-D), (c) *ω*B97X-D, (d) PBE(-D). Dispersion corrections on B3LYP, M06−2X, and PBE values were calculated according to the Grimme D2- and D3-schemes. All cluster calculations were performed using the 6-31+g(d) basis set. Periodic results (PBE-D2 pbc) were obtained using a kinetic energy cutoff of 600 eV. [a]Experimental values from ref 14.

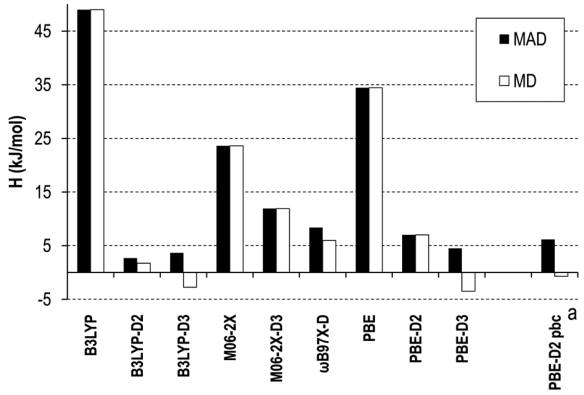

Figure 6. Mean deviation (MD) and mean absolute deviation (MAD) between theoretical and experimental adsorption enthalpies. [a]Based on the reduced data set for which periodic results were available.

deviation (MD) and mean absolute deviation (MAD) between theoretical and experimental values. Dispersion-corrected functionals are clearly essential to obtain reliable trends for the adsorption enthalpies. B3LYP and PBE perform very poorly, exhibiting a mean absolute deviation of 49 and 34 kJ/mol, respectively, when comparing calculated and experimental adsorption enthalpies at 400 K. For M06−2X, a slightly better result is obtained (MAD of 24 kJ/mol), which is mainly due to the reasonable performance for the smallest adsorbates (cf. supra). The results improve substantially by adding dispersion corrections, reducing MADs to 3−4, 5−7, and 12 kJ/mol for B3LYP-D, PBE-D, and M06−2X-D respectively. *ω*B97X-D performs generally well across the entire series of alcohols and nitriles (MAD of 8 kJ/mol). MADs for PBE-D values obtained using periodic calculations (6 kJ/mol) and using the cluster approach (7 kJ/mol) are comparable, confirming that periodic simulations do not offer a substantial advantage. The adsorbates for which the adsorption enthalpies could not be determined

dx.doi.org/10.1021/jp2123828 | J. Phys. Chem. C 2012, 116, 5499−5508

based on the periodic model (i.e., propanol and isobutyronitrile) were excluded in the calculation of the MD and MAD values for the periodic PBE-D results.

3.4. Framework–Adsorbate Interplay. The total heat of adsorption of the alcohols or nitriles results from the interplay of different effects: on one hand, the adsorption complex is stabilized by hydrogen bonds and dispersive interactions with the zeolite walls; on the other hand, deformations of both the zeolite host and the adsorbate molecule have a destabilizing effect. Calculating the different contributions separately provides a more detailed insight into their relative importance.

The interactions between adsorbate and the zeolite (ΔE_{inter}) can be calculated from

$$\Delta E_{inter} = E_{complex} - E^{c}_{zeolite} - E^{c}_{adsorbate}$$

Herein, energies of the zeolite and adsorbate are evaluated at the geometries found in the adsorption complex without further optimization (denoted by the superscript 'c'). As a result, contributions due to deformation of the zeolite host and the adsorbate are excluded. These can be calculated separately from

$$\Delta E^{zeo}_{deform} = E^{c}_{zeolite} - E_{zeolite}$$

$$\Delta E^{ads}_{deform} = E^{c}_{adsorbate} - E_{adsorbate}$$

The total adsorption energy (ΔE_{ads}) is now given by

$$\Delta E_{ads} = \Delta E_{inter} + \Delta E^{zeo}_{deform} + \Delta E^{ads}_{deform}$$

The various contributions at the B3LYP-D level of theory are listed in Table 3. Note that these are purely electronic energies, differing slightly from the adsorption enthalpies at 400 K presented in Table 2.

Table 3. Different Contributions to the Adsorption Energy[a]

	ΔE_{inter}	ΔE^{zeo}_{deform}	ΔE^{ads}_{deform}	ΔE_{ads}
H_2O	−109.0	10.3	1.0	−97.7
CH_3OH	−135.1	14.6	1.6	−118.9
CH_3CH_2OH	−156.2	15.8	2.3	−138.1
$CH_3(CH_2)_2OH$	−177.3	17.1	1.7	−158.5
CH_3CN	−118.3	2.9	0.3	−115.2
CH_3CH_2CN	−140.6	6.8	0.5	−133.3
$CH_3(CH_2)_2CN$	−159.2	6.2	2.2	−150.8
$(CH_3)_2CHCN$	−154.7	8.7	0.6	−145.4

[a] ΔE_{inter}: interaction between zeolite and adsorbate. ΔE^{zeo}_{deform}: deformation of the zeolite host. ΔE^{ads}_{deform}: deformation of the adsorbate. ΔE_{ads}: total adsorption energy. Level of theory: B3LYP-D/6-31+g(d). All values in kJ/mol.

While the interaction between the zeolite host and the adsorbate molecules dominates the final adsorption energy, destabilization due to deformation of the zeolite host clearly increases with increasing size of the adsorbate molecule and is generally more prominent for water and the alcohols (10–17 kJ/mol), compared to the nitriles (3–9 kJ/mol). The latter could be due to the stronger hydrogen bond interactions between two hydroxyl groups in the case of the alcohols, compared to the somewhat weaker hydrogen bond between the cyanide and zeolite hydroxyl group formed upon nitrile adsorption. A stronger hydrogen bond results in slightly more local deformation of the framework surrounding the active site. Destabilization due to deformation of the adsorbate molecule is virtually negligible for the alcohols and nitriles considered in this study (less than 3 kJ/mol), in agreement with the earlier conclusion that the current adsorbates are not yet hindered by confinement effects in the zeolite pore (cf. Section 3.1).

4. CONCLUSIONS

Adsorption enthalpies of a series of alcohols and nitriles on the zeolite catalyst H-ZSM-5 were calculated using different DFT-based methods. Water, methanol, ethanol, propanol, acetonitrile, propionitrile, butyronitrile, and isobutyronitrile were selected based on the availability of experimental reference data for their differential heats of adsorption in H-ZSM-5, which makes them ideally suited for benchmarking computational methodologies. In addition, the adsorption of weak bases in acidic zeolite materials is a crucial step for many industrial processes, such as the MTO conversion.

Large-cluster calculations on the adsorption complexes indicate that all adsorbates are found to be physisorbed in the H-ZSM-5 cluster, in agreement with experimental IR data for low adsorbate coverage in H-ZSM-5. The alcohols form two and the nitriles one hydrogen bond with the bridging Brønsted acid sites. It was moreover shown that deformation of the zeolite host has a non-negligible destabilizing effect, which increases with the size of the adsorbate molecule and is more prominent for alcohols than for nitriles, as the former interact more strongly with the zeolite.

The performance of different DFT-methods, i.e., B3LYP(-D), PBE(-D), M062X(-D), and ωB97X-D, to reproduce the experimental adsorption enthalpies was assessed, with special emphasis on the influence of dispersion interactions. A proper account of dispersion interactions was found to be indispensable to describe the experimental trend across a series of adsorbates of increasing size, i.e., an increase in adsorption enthalpy by 10–15 kJ/mol for each additional carbon atom. The well-known B3LYP and PBE functionals are completely inadequate to determine adsorption enthalpies for the alcohols and nitriles and are effectively unable to distinguish between alcohols or nitriles of different size. M06–2X, which was parametrized to include weak interactions, was still found to underestimate the adsorption enthalpy for the adsorbates considered in this study. Moreover, the deviation from the experimental trend increases with increasing adsorbate size. For all three functionals, however, the deficiency can be remedied by adding dispersion correction terms as proposed by Grimme. The recent ωB97X-D functional, which combines custom parametrization with Grimme-like dispersion terms, was found to perform well for the calculation of adsorption enthalpies across the series of compounds. Comparing calculated with experimental adsorption enthalpies, B3LYP-D, PBE-D, and ωB97X-D all result in MAD values below 8 kJ/mol for the complete set of alcohols and nitriles.

Comparison with periodic simulations using the PBE-D functional on the full H-ZSM-5 unit cell confirmed that the extended-cluster model offers an attractive alternative, resulting in virtually identical final adsorption enthalpies while avoiding both the larger computational expense and technical difficulties associated with periodic calculations.

■ ASSOCIATED CONTENT

Supporting Information

Complete Gaussian references, convergence criteria used in periodic simulations, critical hydrogen bond lengths and angles for all adsorption complexes, OH-stretch frequency shifts vs gas

dx.doi.org/10.1021/jp2123828 | J. Phys. Chem. C 2012, 116, 5499–5508

phase proton affinities for selected adsorbates, additional figures, and complete coordinates of all optimized adsorption complexes. This material is available free of charge via the Internet at http://pubs.acs.org.

AUTHOR INFORMATION

Corresponding Author

*E-mail: veronique.vanspeybroeck@ugent.be.

Notes

The authors declare no competing financial interest.

ACKNOWLEDGMENTS

This work was supported by the Fund for Scientific Research Flanders (FWO), the Research Board of Ghent University (BOF), and BELSPO in the frame of IAP/6/27. Funding was also received from the European Research Council under the European Community's Seventh Framework Programme [FP7(2007-2013) ERC grant agreement number 240483]. Computational resources and services used in this work were provided by Ghent University.

REFERENCES

(1) *Zeolites for Cleaner Technologies*; Guisnet, M., Gilson, J.-P., Eds.; Imperial College Press: London, 2002; *Vol. 3*.
(2) Stocker, M.; Weitkamp, J. *Microporous Mesoporous Mater.* **1999**, *29*, 1−1.
(3) Haw, J. F.; Song, W.; Marcus, D. M.; Nicholas, J. B. *Acc. Chem. Res.* **2003**, *36*, 317−326.
(4) Svelle, S.; Arstad, B.; Kolboe, S.; Swang, O. *J. Phys. Chem. B* **2003**, *107*, 9281−9289.
(5) Svelle, S.; Kolboe, S.; Olsbye, U.; Swang, O. *J. Phys. Chem. B* **2003**, *107*, 5251−5260.
(6) Svelle, S.; Kolboe, S.; Swang, O. *J. Phys. Chem. B* **2004**, *108*, 2953−2962.
(7) Lesthaeghe, D.; Horre, A.; Waroquier, M.; Marin, G. B.; Van Speybroeck, V. *Chem.—Eur. J.* **2009**, *15*, 10803−10808.
(8) Lesthaeghe, D.; Van der Mynsbrugge, J.; Vandichel, M.; Waroquier, M.; Van Speybroeck, V. *ChemCatChem* **2011**, *3*, 208−212.
(9) McCann, D. M.; Lesthaeghe, D.; Kletnieks, P. W.; Guenther, D. R.; Hayman, M. J.; Van Speybroeck, V.; Waroquier, M.; Haw, J. F. *Angew. Chem., Int. Ed.* **2008**, *47*, 5179−5182.
(10) Hemelsoet, K.; Nollet, A.; Vandichel, M.; Lesthaeghe, D.; Van Speybroeck, V.; Waroquier, M. *ChemCatChem* **2009**, *1*, 373−378.
(11) Hemelsoet, K.; Nollet, A.; Van Speybroeck, V.; Waroquier, M. *Chem.—Eur. J.* **2011**, *17*, 9083−9093.
(12) Van Speybroeck, V.; Van der Mynsbrugge, J.; Vandichel, M.; Hemelsoet, K.; Lesthaeghe, D.; Ghysels, A.; Marin, G. B.; Waroquier, M. *J. Am. Chem. Soc.* **2011**, *133*, 888−899.
(13) Svelle, S.; Tuma, C.; Rozanska, X.; Kerber, T.; Sauer, J. *J. Am. Chem. Soc.* **2009**, *131*, 816−825.
(14) Lee, C. C.; Gorte, R. J.; Farneth, W. E. *J. Phys. Chem. B* **1997**, *101*, 3811−3817.
(15) Denayer, J. F.; Souverijns, W.; Jacobs, P. A.; Martens, J. A.; Baron, G. V. *J. Phys. Chem. B* **1998**, *102*, 4588−4597.
(16) Arik, I. C.; Denayer, J. F.; Baron, G. V. *Microporous Mesoporous Mater.* **2003**, *60*, 111−124.
(17) De Moor, B. A.; Reyniers, M. F.; Marin, G. B. *Phys. Chem. Chem. Phys.* **2009**, *11*, 2939−2958.
(18) De Moor, B. A.; Reyniers, M.-F. o.; Gobin, O. C.; Lercher, J. A.; Marin, G. B. *J. Phys. Chem. C* **2011**, *115*, 1204−1219.
(19) Tuma, C.; Sauer, J. *Phys. Chem. Chem. Phys.* **2006**, *8*, 3955−3965.
(20) Tuma, C.; Sauer, J. *Chem. Phys. Lett.* **2004**, *387*, 388−394.
(21) Tuma, C.; Sauer, J. *Angew. Chem., Int. Ed.* **2005**, *44*, 4769−4771.
(22) Nguyen, C. M.; Reyniers, M. F.; Marin, G. B. *Phys. Chem. Chem. Phys.* **2010**, *12*, 9481−9493.
(23) Nguyen, C. M.; Reyniers, M. F.; Marin, G. B. *J. Phys. Chem. C* **2011**, *115*, 8658−8669.
(24) De Moor, B. A.; Reyniers, M.-F. o.; Sierka, M.; Sauer, J.; Marin, G. B. *J. Phys. Chem. C* **2008**, *112*, 11796−11812.
(25) De Moor, B. A.; Ghysels, A.; Reyniers, M.-F. o.; Van Speybroeck, V.; Waroquier, M.; Marin, G. B. *J. Chem. Theory Comput.* **2011**, *7*, 1090−1101.
(26) Hohenberg, P.; Kohn, W. *Phys. Rev.* **1964**, *136*, B864.
(27) Kohn, W.; Sham, L. J. *Phys. Rev.* **1965**, *140*, A1133.
(28) Grimme, S. *J. Comput. Chem.* **2004**, *25*, 1463−1473.
(29) Grimme, S.; Antony, J.; Schwabe, T.; Muck-Lichtenfeld, C. *Org. Biomol. Chem.* **2007**, *5*, 741−758.
(30) Becke, A. D. *J. Chem. Phys.* **1993**, *98*, 5648−5652.
(31) Lee, C.; Yang, W.; Parr, R. G. *Phys. Rev. B* **1988**, *37*, 785.
(32) Grafenstein, J.; Cremer, D. *J. Chem. Phys.* **2009**, *130*, 124105.
(33) Johnson, E. R.; Mackie, I. D.; DiLabio, G. A. *J. Phys. Org. Chem.* **2009**, *22*, 1127−1135.
(34) Sato, T.; Nakai, H. *J. Chem. Phys.* **2009**, *131*, 224104.
(35) Goerigk, L.; Grimme, S. *Phys. Chem. Chem. Phys.* **2011**, *13*, 6670−6688.
(36) Grimme, S.; Antony, J.; Schwabe, T.; Muck-Lichtenfeld, C. *Org. Biomol. Chem.* **2007**, *5*, 741−758.
(37) Grimme, S.; Antony, J.; Ehrlich, S.; Krieg, H. *J. Chem. Phys.* **2010**, *132*, 154104.
(38) Zhao, Y.; Truhlar, D. G. *Theor. Chem. Acc.* **2008**, *120*, 215−241.
(39) Zhao, Y.; Truhlar, D. G. *Acc. Chem. Res.* **2008**, *41*, 157−167.
(40) Catak, S.; D'Hooghe, M.; De Kimpe, N.; Waroquier, M.; Van Speybroeck, V. *J. Org. Chem.* **2010**, *75*, 885−896.
(41) Catak, S.; Hemelsoet, K.; Hermosilla, L.; Waroquier, M.; Van Speybroeck, V. *Chem.—Eur. J.* **2011**, *17*, 12027−12036.
(42) Boekfa, B.; Choomwattana, S.; Khongpracha, P.; Limtrakul, J. *Langmuir* **2009**, *25*, 12990−12999.
(43) Boekfa, B.; Pantu, P.; Probst, M.; Limtrakul, J. *J. Phys. Chem. C* **2010**, *114*, 15061−15067.
(44) Grimme, S. *J. Comput. Chem.* **2006**, *27*, 1787−1799.
(45) Chai, J.-D.; Head-Gordon, M. *Phys. Chem. Chem. Phys.* **2008**, *10*, 6615−6620.
(46) Zecchina, A.; Spoto, G.; Bordiga, S. *Phys. Chem. Chem. Phys.* **2005**, *7*, 1627−1642.
(47) Haase, F.; Sauer, J. *J. Am. Chem. Soc.* **1995**, *117*, 3780−3789.
(48) Krossner, M.; Sauer, J. *J. Phys. Chem.* **1996**, *100*, 6199−6211.
(49) Sauer, J.; Ugliengo, P.; Garrone, E.; Saunders, V. R. *Chem. Rev.* **1994**, *94*, 2095−2160.
(50) Blaszkowski, S. R.; van Santen, R. A. *J. Phys. Chem.* **1995**, *99*, 11728−11738.
(51) Hemelsoet, K.; Ghysels, A.; Mores, D.; De Wispelaere, K.; Van Speybroeck, V.; Weckhuysen, B. M.; Waroquier, M. *Catal. Today* **2011**, *177*, 12−24.
(52) Jentys, A.; Warecka, G.; Derewinski, M.; Lercher, J. A. *J. Phys. Chem.* **1989**, *93*, 4837−4843.
(53) Mirth, G.; Lercher, J. A.; Anderson, M. W.; Klinowski, J. *J. Chem. Soc., Faraday Trans.* **1990**, *86*, 3039−3044.
(54) Zecchina, A.; Bordiga, S.; Spoto, G.; Scarano, D.; Spano, G.; Geobaldo, F. *J. Chem. Soc., Faraday Trans.* **1996**, *92*, 4863−4875.
(55) Pelmenschikov, A. G.; van Santen, R. A.; Janchen, J.; Meijer, E. *J. Phys. Chem.* **1993**, *97*, 11071−11074.
(56) Pelmenschikov, A. G.; van Wolput, J. H. M. C.; Jaenchen, J.; van Santen, R. A. *J. Phys. Chem.* **1995**, *99*, 3612−3617.
(57) Florian, J.; Kubelkova, L. *J. Phys. Chem.* **1994**, *98*, 8734−8741.
(58) Kubelkova, L.; Kotrla, J.; Florian, J. *J. Phys. Chem.* **1995**, *99*, 10285−10293.
(59) Trombetta, M.; Armaroli, T.; Alejandre, A. G.; Solis, J. R.; Busca, G. *Appl. Catal., A* **2000**, *192*, 125−136.
(60) Simperler, A.; Bell, R. G.; Foster, M. D.; Gray, A. E.; Lewis, D. W.; Anderson, M. W. *J. Phys. Chem. B* **2004**, *108*, 7152−7161.
(61) van Koningsveld, H. *Acta Crystallogr., Sect. B: Struct. Sci.* **1990**, *46*, 731−735.
(62) Lesthaeghe, D.; Van Speybroeck, V.; Waroquier, M. *Phys. Chem. Chem. Phys.* **2009**, *11*, 5222−5226.

(63) Bhan, A.; Joshi, Y. V.; Delgass, W. N.; Thomson, K. T. *J. Phys. Chem. B* **2003**, *107*, 10476−10487.
(64) Alvarado-Swaisgood, A. E.; Barr, M. K.; Hay, P. J.; Redondo, A. *J. Phys. Chem.* **1991**, *95*, 10031−10036.
(65) Lonsinger, S. R.; Chakraborty, A. K.; Theodorou, D. N.; Bell, A. T. *Catal. Lett.* **1991**, *11*, 209−217.
(66) Redondo, A.; Hay, P. J. *J. Phys. Chem.* **1993**, *97*, 11754−11761.
(67) Grau-Crespo, R.; Peralta, A. G.; Ruiz-Salvador, A. R.; Gomez, A.; Lopez-Cordero, R. *Phys. Chem. Chem. Phys.* **2000**, *2*, 5716−5722.
(68) Sklenak, S.; Dedecek, J.; Li, C.; Wichterlova, B.; Gabova, V.; Sierka, M.; Sauer, J. *Phys. Chem. Chem. Phys.* **2009**, *11*, 1237−1247.
(69) Sklenak, S.; Dedecek, J.; Li, C.; Wichterlova, B.; Gabova, V.; Sierka, M.; Sauer, J. *Angew. Chem., Int. Ed.* **2007**, *46*, 7286−7289.
(70) Dedecek, J.; Kaucky, D.; Wichterlova, B. *Chem. Commun. (Cambridge, U. K.)* **2001**, 970−971.
(71) Baba, T.; Komatsu, N.; Ono, Y.; Sugisawa, H. *J. Phys. Chem. B* **1998**, *102*, 804−808.
(72) Ryder, J. A.; Chakraborty, A. K.; Bell, A. T. *J. Phys. Chem. B* **2000**, *104*, 6998−7011.
(73) Franke, M. E.; Sierka, M.; Simon, U.; Sauer, J. *Phys. Chem. Chem. Phys.* **2002**, *4*, 5207−5216.
(74) Frisch, M. J.; et al., *Gaussian 03*, revision E.01 ed.; Gaussian, Inc.: Wallingford CT, 2004.
(75) Frisch, M. J.; et al., *Gaussian 09*, revision A.02 ed.; Gaussian, Inc.: Wallingford CT, 2009.
(76) Grimme, S., http://toc.uni-muenster.de/DFTD3/.
(77) Kresse, G.; Furthmuller, J. *Phys. Rev. B* **1996**, *54*, 11169.
(78) Kresse, G.; Furthmuller, J. *Comput. Mater. Sci.* **1996**, *6*, 15−50.
(79) Kresse, G.; Hafner, J. *Phys. Rev. B* **1993**, *47*, 558.
(80) Kresse, G.; Hafner, J. *Phys. Rev. B* **1994**, *49*, 14251.
(81) Perdew, J. P.; Burke, K.; Ernzerhof, M. *Phys. Rev. Lett.* **1996**, *77*, 3865.
(82) Perdew, J. P.; Burke, K.; Ernzerhof, M. *Phys. Rev. Lett.* **1997**, *78*, 1396.
(83) Blochl, P. E. *Phys. Rev. B* **1994**, *50*, 17953.
(84) Structure Commision of the International Zeolite Association (IZA-SC), Database of Zeolite Structures, http://www.iza-structure.org/databases/.
(85) CMM Code, http://molmod.ugent.be/code/wiki.
(86) Ghysels, A.; Verstraelen, T.; Hemelsoet, K.; Waroquier, M.; Van Speybroeck, V. *J. Chem. Inf. Model.* **2010**, *50*, 1736−1750.
(87) Fermann, J. T.; Moniz, T.; Kiowski, O.; McIntire, T. J.; Auerbach, S. M.; Vreven, T.; Frisch, M. J. *J. Chem. Theory Comput.* **2005**, *1*, 1232−1239.
(88) Merrick, J. P.; Moran, D.; Radom, L. *J. Phys. Chem. A* **2007**, *111*, 11683−11700.
(89) Gilli, P.; Bertolasi, V.; Ferretti, V.; Gilli, G. *J. Am. Chem. Soc.* **1994**, *116*, 909−915.
(90) Sierka, M.; Sauer, J. *J. Phys. Chem. B* **2001**, *105*, 1603−1613.
(91) Vandichel, M.; Lesthaeghe, D.; Van der Mynsbrugge, J.; Waroquier, M.; Van Speybroeck, V. *J. Catal.* **2010**, *271*, 67−78.